Appl. Phys. A 89, 115–119 (2007)
DOI: 10.1007/s00339-007-4180-9

Applied Physics A
Materials Science & Processing

ZHE ZHENG[1]
YUNZHONG CHEN[2]
ZEXIANG SHEN[1]
JAN MA[2]
CHORNG-HAUR SOW[3,4]
WEI HUANG[5]
TING YU[1,✉]

Ultra-sharp α-Fe_2O_3 nanoflakes: growth mechanism and field-emission

[1] Division of Physics and Applied Physics, School of Physical and Mathematical Sciences, Nanyang Technological University, 1 Nanyang Walk, Block 5, 637616 Singapore
[2] School of Materials Science and Engineering, Nanyang Technological University, 1 Blk N4.1, 50 Nanyang Avenue, 639798 Singapore
[3] Department of Physics, National University of Singapore, 2 Science Drive 3, 117542 Singapore
[4] National University of Singapore Nanoscience and Nanotechnology Initiative, Blk S13, Science Drive 3, 117542 Singapore
[5] Institute of Advanced Materials (IAM), Fudan University, 220 Handan Road, Shanghai 200433, P.R. China

Received: 28 March 2007/Accepted: 14 June 2007
Published online: 26 June 2007 •

ABSTRACT We report the synthesis of single-crystalline α-Fe_2O_3 nanoflakes from a simple Fe–air reaction within the temperatures range of 260–400 °C. The nanoflakes synthesized at the lowest temperature (260 °C) in this work show an ultra-sharp morphology: 5–10 nm in thickness, 1–2 μm in length, 20 nm in base-width and around 5 nm at the tips; successfully demonstrate the promising electron field emission properties of a large-scaled α-Fe_2O_3 nanostructure film and exhibit the potential applications as future field-emission (FE) electron sources and displays (FEDs). The formation and growth of α-Fe_2O_3 nanostructures were discussed based on the surface diffusion mechanism.

PACS 79.60.Jv; 79.70.+q; 77.84.Bw

1 Introduction

One-dimensional (1D) and quasi-one-dimensional nanostructures exhibit promising properties and potential applications in magneto-electronic devices [1], room temperature UV-lasing devices [2] and high-density information storage devices [3]. Many methods have been developed for the fabrication of 1D nanostructure arrays, including template methods [4] and catalytic growth [5]. Since the sharp tips of 1D nanostructures can effectively enhance local electric fields, using them as field emission cathodes is a promising way to obtain high brightness electron sources and to fabricate field emission displays (FEDs) [6]. With the properties like low turn on field, high current density and high enhancement factor, metal oxide nanostructures play an important role in the family of candidates for field emission [7, 8]. There is on-going interest to find innovative ways to fabricate metal-oxide-based 1D nanostructure at low cost and in a simple manner.

Iron oxide is one of the most important magnetic materials and shows numerous potential applications, such as the active component of gas sensors [9], photocatalyst [10] and enzyme immunoassay [11, 12]. As the most stable phase among the iron oxides under ambient condition, α-Fe_2O_3 (hematite), a semiconductor ($E_g = 2.1$ eV) material has attracted great attentions [13]. The previous works have lowered the growth temperatures of 1D α-Fe_2O_3 nanostructures ranged from 800 to 400 °C [13, 14] but some methods are still rather complicated. For example, Fu et al. [15] synthesized hematite nanowire arrays by heating Fe foil in a special oxidization atmosphere: a gas mixture of CO_2 (19.30%, in volume), SO_2 (0.14%), NO_2 (80.56%) and some H_2O vapor. To successfully synthesize nanowires, the pressure and the flow rate of the gas mixture were precisely controlled.

✉ Fax: +65 67941325, E-mail: yuting@ntu.edu.sg

More recently, we developed a simple and efficient method to fabricate metal oxide nanostructures by heating the metal foil or films on a hotplate in air [7, 8, 16]. Using this method, we successfully synthesized the α-Fe_2O_3 nanoflakes on a wide range of substrates at 300 °C in air [8]. Such α-Fe_2O_3 nanoflakes grown on sharp *W* tips [8] and atomic force microscope (AFM) tips [17] exhibit promising electron field emission properties. Unfortunately, we failed to observe an effective field induced electron emission for a large scale film sample which has more potential applications. In this work, we expand the heating temperatures into the range of 260–400 °C. The results demonstrate that the temperature parameters strongly affect the growth processes and the final morphologies of the α-Fe_2O_3 nanoflakes. More importantly, the ultra-sharp nanoflakes synthesized at 260 °C, to date, the lowest growth temperature of such heat-oxide methods, exhibits promising electron field emission properties in a large scale. The growth mechanism of the α-Fe_2O_3 nanoflakes was also discussed in this report.

2 Experimental

Experimentally, fresh iron foils ($10 \times 10 \times 0.25$ mm) with a purity of 99.9% (Aldrich) were used as both reagents and substrates for the growth of α-Fe_2O_3 nanoflakes. The cleaned Fe foil was heated on a hotplate under ambient conditions. The growth temperatures were varied from 260 °C to 400 °C and the growth duration was fixed as 10 h. After being cooled down

to room temperature naturally, the morphologies of the as-prepared products were examined by scanning electron microscopy (SEM) (JEOL JSM-6700F) for the topographical morphologies; the compositions of the top surface were characterized by X-ray diffraction (XRD) (Bruker D8 with Cu K_α irradiation) and micro-Raman spectroscopy (Witech CRM200, $\lambda_{\text{laser}} = 532$ nm). The transmission electron microscopic (TEM) (JEOL JEM 2010F, 200 kV) observation shows the crystal structure of the ultra-sharp nanoflake products. Field-emission measurement was carried out in a vacuum chamber with a pressure of 5.8×10^{-7} Torr at room temperature under a two-parallel-plate configuration. Details of the measurement system and procedure were reported previously [18].

3 Results and discussion

Figure 1 shows the SEM images of the as-prepared samples obtained by heating iron foils on a hotplate with different temperatures (260–400 °C) and fixed duration (10 h). Clearly, the flakes become broader with increasing the reaction temperatures, indicating the obvious heating temperature's effect on the morphologies of the nanostructures. To further quantify this effect, the sharpness of the nanoflakes with different growth temperatures were investigated based on the high magnification SEM images. The sharpness of the nanoflake was measured by two ways in this work: one is the radius of curvature at the nanoflake tip and the other is the aspect ratio of L/FWHL (L is the length of nanoflake and FWHL is the full width of the half length). As shown in Fig. 2, the lower heating temperatures dramatically increase the sharpness of flakes as indicated by the higher aspect ratio and smaller radius. In general, the random aligned nanoflakes synthesized at the lowest temperature, 260 °C are about 5–10 nm in thickness, 20 nm at the bases, 5 nm at the tips and 1–2 μm in length. Comparing with the flakes formed (300 °C, 24 h) in our previous work [8], the nanoflakes synthesized in this work show an ultra-sharp needle-like shape and a lower density which may effectively enhance the field induced electron emission from such nanoflake film.

Figure 3a shows the XRD pattern of the as-prepared sample. Two phases of iron oxide, α-Fe_2O_3 and Fe_3O_4 were formed by heating Fe foil in air at 260 °C. The peaks corresponding to the rhombohedral α-Fe_2O_3 with lattice constants $a = 5.035$ Å and $c = 13.749$ Å is able to be readily conformed from XRD pattern [19]. It was also noted that, comparing with the standard powder diffraction pattern of bulk α-Fe_2O_3, our XRD pattern of the α-Fe_2O_3 nanoflakes

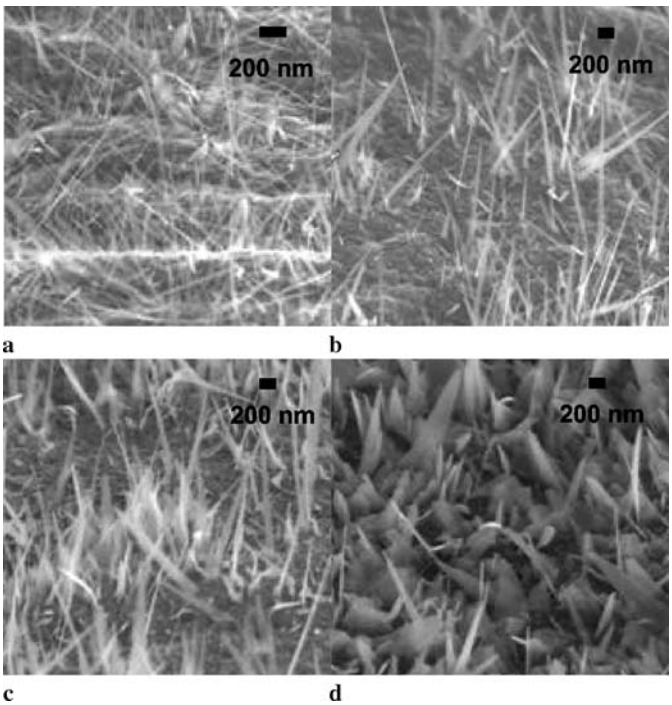

FIGURE 1 SEM images of the top surfaces of Fe foils heated for 10 h at (**a**) 260 °C, (**b**) 300 °C, (**c**) 350 °C and (**d**) 400 °C

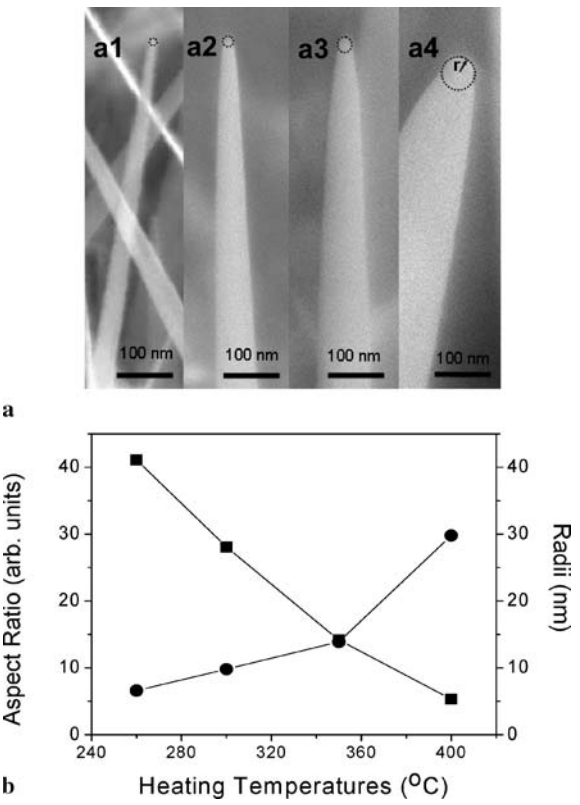

FIGURE 2 (**a1**–**a4**) High magnification SEM images of the nanoflakes synthesized at 260, 300, 350, and 400 °C, respectively. (**b**) Aspect ratio (*solid squires*) defined as length over full width at half length and radii (*solid circles*) of tangent circles of the tips as a function of heating temperatures

exhibits a much higher ratio of the intensity of the (110) planes' diffraction peak to the intensity of the (104) planes' (2.5, nanoflakes vs 0.76, powder [19]). This may indicate a favorable growth plane exists, as evidenced by our TEM results discussed below. The Raman spectrum of the top surface of the as-prepared sample is shown in Fig. 3b. Seven peaks present in the range of 150–800 cm^{-1}. The peaks locating at 225, 245, 291, 408 and 499 cm^{-1} correspond to the α-Fe_2O_3 phase [20], namely two A_{1g} modes (225 and 499 cm^{-1}) and three E_g modes (245, 291 and 408 cm^{-1}). Those peaks locating at 552 and 671 cm^{-1} correspond to the Fe_3O_4 [21], namely T_{2g} mode (552 cm^{-1}) and A_{1g} mode (671 cm^{-1}).

The TEM was employed to further confirm the composition and the crystal structure of the ultra-sharp nanoflakes. Figure 4a shows the typical TEM image of α-Fe_2O_3 nanoflake. As can be seen in the high resolution TEM (HRTEM) image (Fig. 4b) of the region highlighted by a circle in Fig. 4a, the fringe spacing of 0.252 nm concurs well with the interplanar spacing of the plane (110) [19]. The selected area electron diffraction (SAED) pattern of the flake is shown in Fig. 4c. The growth direction of the nanoflakes was [110], which is consistent with our previous study [17].

Considering the growth temperatures (260–400 °C) are much lower than the melting points of Fe and α-Fe_2O_3 (1535 and 1350 °C, respectively) [15], the growth of α-Fe_2O_3 nanoflakes is inexplicable by the vapor phase mechanism such as the vapor–liquid–solid (VLS) and vapor–solid (VS) processes [13]. In our work, we attributed the growth mechanism to the surface diffusion of iron atoms and iron oxide molecules. A schematic view of the formation of α-Fe_2O_3 nanoflakes is shown in Fig. 5. Initially, the top layer of Fe foil was oxidized by the oxygen molecules in air and formed a very thin layer of mixture of α-Fe_2O_3 and Fe_3O_4. With continuous heating, the Fe_3O_4 at the very top layer was further oxidized to α-Fe_2O_3 and another layer of Fe_3O_4 below the thin top layer of α-Fe_2O_3 was formed by the reaction between oxygen diffusing through the thin top layer and the Fe substrate. During the formation and growth of the α-Fe_2O_3 layer, substantial stresses were expected to accumulate. Once a critical limit was reached, the stresses were relaxed by slipping in α-Fe_2O_3 crystals and the screw dislocations might be produced. When the dislocations were generated along an appropriate crystal direction, Fe atoms and iron oxide molecules adsorbed on the surface began to migrate toward and stack in the corresponding plane to maintain a flake shape [22]. Considering the crystal structure of α-Fe_2O_3, we find that the preferential migration direction, especially at the lower heating temperatures (for example 260 °C), may be [110] and the growth plane may be (110) where the oxygen is rich and Fe is deficient [13]. Driven by the O-rich and Fe-deficient, at low temperatures (260–300 °C), the diffusion of Fe atoms and oxide molecules along the [110] direction is more facile so that the growth is mainly along the [110] direction named as the axis growth [22], which resulted in the large aspect ratio (> 40) as shown in Fig. 2b. At higher temperatures (350–400 °C), the diffusion in other crystal directions may be enhanced and the radial growth occurred. This resulted in the broaden-

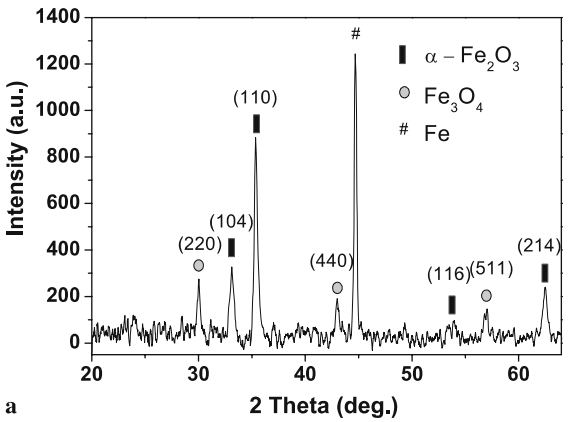

FIGURE 3 (**a**) XRD pattern and (**b**) Raman spectrum of the as-prepared sample shown in Fig. 1a

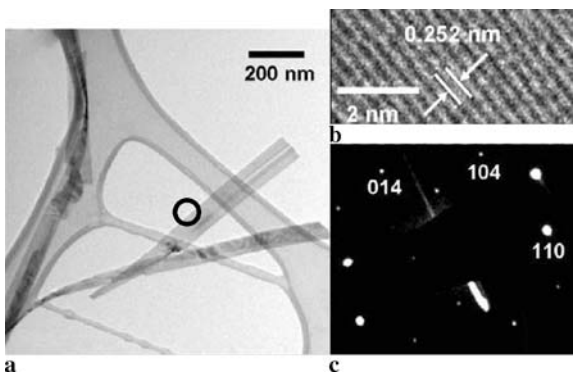

FIGURE 4 (**a**) TEM image of the α-Fe_2O_3 nanoflakes, (**b**) HRTEM image of the nanoflakes and (**c**) the electron diffraction pattern (*circled region*) of nanoflakes showing the good agreement with the diffraction pattern of α-Fe_2O_3 from the zone axis of [$\bar{4}$41]

ing of nanoflakes and small aspect ratio (≤ 10).

Considering their ultra-sharp morphology, we studied the field-emission properties of the α-Fe_2O_3 nanoflakes film synthesized at 260 °C for 10 h. Figure 6 shows the typical current density–electric field (J–E) curve. The exponential dependence between the emission current and the applied field, plotted in $\ln(J/E^2) \sim 1/E$ relationship inset of Fig. 6, indicates that the field emission from α-Fe_2O_3 ultra-sharp nanoflakes films follows the Fowler–Nordheim (FN) relationship [23]. The dots are experimental data and the solid line is the fitting curve according to the simplified Fowler–Nordheim equation:

$$J = \frac{A(\beta E)^2}{\varphi} \exp\left[-\frac{B\varphi^{\frac{3}{2}}}{\beta E}\right], \qquad (1)$$

where J is the current density, E is the applied field strength, φ is the work function, for electron emission which is estimated to be 5.4 eV [24] for α-Fe_2O_3, A and B are constants with the value of 1.54×10^{-6} (A V^{-2} eV) and 6.83×10^7 (V cm^{-1} eV$^{-3/2}$) [17], respectively. Here, β is the field enhancement factor, which is defined by:

$$E_{\text{local}} = \beta E = \beta \frac{V}{d}, \qquad (2)$$

where E_{local} is the local electric field nearby the emitter tip, d is the average spacing between the electrodes (d = 100 μm in this work) and V is the applied voltage. For the α-Fe_2O_3 ultra-sharp nanoflakes with the lowest growth temperature (260 °C), β was obtained to be 1131 from the linear fitting of the F–N curve and the turn-on field was measured to be about 7.2 V/μm (Fig. 6). Compared to the AlN nanoneedles ($\beta = 950$) [25], $NiSi_2$ nanorods ($\beta = 630$) [26], $TiSi_2$ nanowires ($\beta = 501$) [27] and the α-Fe_2O_3 nanowires ($\beta = 560$ and 1500) [28], such an enhancement factor is acceptable for application, although much lower than that of carbon nanotubes [29]. One of the reasons for this low enhancement factor could be the random alignment of the nanoflakes (Fig. 1a). We can also see that at high electric fields the linear relationship between $\ln(J/E^2)$ and $1/E$ suggests that the quantum tunneling mechanism is responsible for the emission from the ultra-sharp nanoflakes [30]. In our previous works [8, 17], the electron field emission was only effectively observed from the α-Fe_2O_3 nanoflakes grown on AFM tips or W tips but not from the film. In this work, the ultra-sharp α-Fe_2O_3 nanoflakes film with a large scale exhibits promising FE properties. This improvement may be because of the ultra-sharp morphology and a lower density which are able to effectively weaken the screening effect, increase the field enhancement factor [18, 31] (shown in Fig. 1) and consequently enhance the FE efficiency.

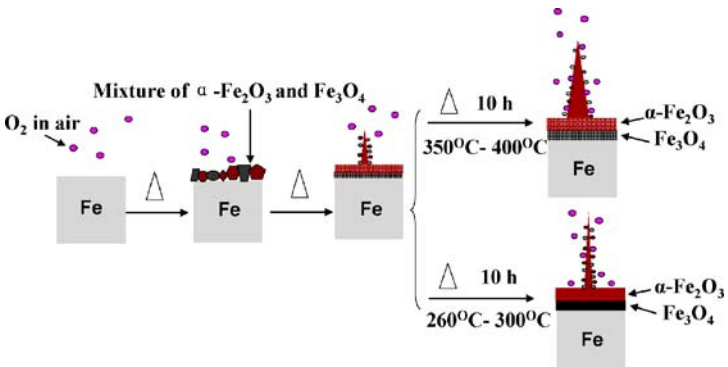

FIGURE 5 A schematic diagram of the formation and growth of α-Fe_2O_3 nanoflakes

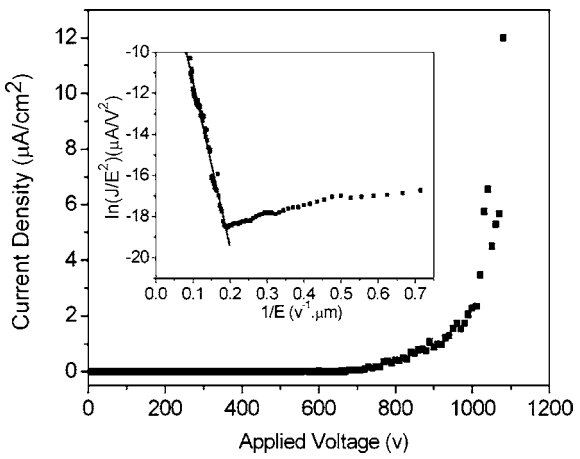

FIGURE 6 Typical field-emission current–voltage (I–V) curves of the α-Fe_2O_3 nanoflakes films synthesized at 260 °C for 10 h. *Inset* shows the F–N plots ($\ln(J/E^2)$ versus $1/E$) accordingly, which exhibits a good linear dependence (*solid line* is the fitting result)

4 Conclusion

In conclusion, single crystalline α-Fe_2O_3 nanoflakes have been synthesized from a rather simple Fe–air reaction at temperatures ranged from 260 °C to 400 °C. A surface diffusion mechanism is proposed to account for the growth of α-Fe_2O_3 nanoflakes. The electron field emission investigations show the ultra-sharp α-Fe_2O_3 nanoflakes films fabricated at a low temperature of 260 °C exhibit promising field emission properties. With further improvements like growth of well aligned ultra-sharp flakes, it is believed that α-Fe_2O_3 nanoflakes could be one of the promising candidates as future field emission electron sources and displays (FEDs).

REFERENCES

1 H. Ohno, Science **281**, 951 (1998)
2 M. Huang, S. Mao, H. Yan, Y. Wu, H. Kind, E. Weber, R. Russo, P.D. Yang, Science **292**, 1897 (2001)
3 W.S. Yun, J.J. Urban, Q. Gu, H. Park, Nano Lett. **2**, 447 (2002)
4 R. Fan, Y.Y. Wu, D.Y. Li, M. Yue, A. Majumdar, P.D. Yang, J. Am. Chem. Soc. **125**, 5254 (2003)
5 X.D. Wang, C.J. Summers, Z.L. Wang, Nano Lett. **4**, 423 (2004)
6 Y. Saito, S. Uemura, Carbon **38**, 169 (2000)
7 T. Yu, Y.W. Zhu, X.J. Xu, Z.X. Shen, P. Chen, C.T. Lim, J.T.L. Thong, C.H. Sow, Adv. Mater. **17**, 1595 (2005)
8 T. Yu, Y.W. Zhu, X.J. Xu, K.S. Yeong, Z.X. Shen, P. Chen, C.T. Lim, J.T.L. Thong, C.H. Sow, Small **2**, 80 (2006)
9 J.S. Han, T. Bredow, D.E. Davey, A.B. Yu, D.E. Mulcahy, Sens. Actuators B **75**, 18 (2001)
10 S.N. Frank, A.J. Bard, J. Phys. Chem. **81**, 1484 (1977)
11 J. Ugelstad, A. Berge, T. Ellingsen, R. Schmid, T.N. Nilsen, P.C. Mørk, P. Stenstad, E. Hornse, Ø. Olsvik, Prog. Polym. Sci. **17**, 87 (1992)

12 X.Y. Liu, X.B. Ding, Z.H. Zheng, Y.X. Peng, A.S.C. Chan, C.W. Yip, X.P. Long, Polym. Int. **52**, 235 (2003)
13 X.G. Wen, S.H. Wang, Y. Ding, Z.L. Wang, S.H. Yang, J. Phys. Chem. B **109**, 215 (2005)
14 Y.M. Zhao, Y.H. Li, R.Z. Ma, M.J. Roe, D.G. McCartney, Y.Q. Zhu, Small **2**, 422 (2006)
15 Y.Y. Fu, R.M. Wang, J. Xu, J. Chen, Y. Yan, A.V. Narlikar, H. Zhang, Chem. Phys. Lett. **379**, 373 (2003)
16 T. Yu, X. Zhao, Z.X. Shen, Y.H. Wu, W.H. Su, J. Cryst. Growth **268**, 590 (2004)
17 Y.W. Zhu, T. Yu, A.T.S. Wee, X.J. Xu, C.T. Lim, J.T.L. Thong, C.H. Sow, Appl. Phys. Lett. **87**, 023 103 (2005)
18 Y.W. Zhu, T. Yu, F.C. Cheong, X.J. Xu, C.T. Lim, V.B.C. Tan, J.T.L. Thong, C.H. Sow, Nanotechnology **16**, 88 (2005)
19 Joint Committee on Powder Diffraction Standards (JCPDS), Card No. 87 1166, hematite (α-Fe_2O_3)
20 I.R. Beattie, T.R. Gilson, J. Chem. Soc. A **5**, 980 (1983)
21 J.L. Verble, Phys. Rev. B **9**, 5236 (1974)
22 R. Takagi, J. Phys. Soc. Japan **12**, 1212 (1957)
23 R. Fowler, L.W. Nordheim, Proc. R. Soc. London A **119**, 173 (1928)
24 V.E. Hendrich, P.A. Cox, in: *Surface Science of Metal Oxides* (Cambridge Univ. Press, Cambridge, 1994)
25 Q. Zhao, J. Xu, X.Y. Xu, Z. Wang, D.P. Yang, Appl. Phys. Lett. **85**, 5331 (2005)
26 Y.W. Ok, T.Y. Seong, C.J. Choi, K.N. Tu, Appl. Phys. Lett. **88**, 043 106 (2006)
27 Q. Xiang, Q.X. Wang, Z. Wang, X.Z. Zhang, L.Q. Liu, J. Xu, D.P. Yu, Appl. Phys. Lett. **86**, 243 103 (2005)
28 Y.L. Chueh, M.W. Lai, J.Q. Liang, L.J. Chou, Z.L. Wang, Adv. Funct. Mater. **16**, 2243 (2006)
29 I. Alexandrou, E. Kymakis, G.A.J. Amaratunga, Appl. Phys. Lett. **80**, 1435 (2002)
30 J.W. Gadzuk, E.W. Plummer, Rev. Mod. Phys. **45**, 487 (1973)
31 J. Zhou, L. Gong, S.Z. Deng, J. Chen, J.C. She, N.S. Xu, R. Yang, Z.L. Wang, Appl. Phys. Lett. **87**, 223 108 (2005)